Chiral recognition in dimerization of adsorbed cysteine observed by scanning tunnelling microscopy

Angelika Kühnle, Trolle R. Linderoth, Bjørk Hammer & Flemming Besenbacher

Interdisciplinary Nanoscience Center at University of Aarhus (iNANO) and Institute of Physics and Astronomy, University of Aarhus, DK-8000 Aarhus C, Denmark

Stereochemistry plays a central role in controlling molecular recognition and interaction: the chemical and biological properties of molecules depend not only on the nature of their constituent atoms but also on how these atoms are positioned in space. Chiral specificity is consequently fundamental in chemical biology and pharmacology[1,2] and has accordingly been widely studied. Advances in scanning probe microscopies now make it possible to probe chiral phenomena at surfaces at the molecular level. These methods have been used to determine the chirality of adsorbed molecules[3–5], and to provide direct evidence for chiral discrimination in molecular interactions[6] and the spontaneous resolution of adsorbates into extended enantiomerically pure overlayers[3,7–9]. Here we report scanning tunnelling microscopy studies of cysteine adsorbed to a (110) gold surface, which show that molecular pairs formed from a racemic mixture of this naturally occurring amino acid are exclusively homochiral, and that their binding to the gold surface is associated with local surface restructuring. Density-functional theory[10] calculations indicate that the chiral specificity of the dimer formation process is driven by the optimization of three bonds on each cysteine molecule. These findings thus provide a clear molecular-level illustration of the well known three-point contact model[11,12] for chiral recognition in a simple bimolecular system.

The mercapto or thiol group -SH binds to gold with high affinity, and a rich literature on the adsorption of self-assembled thiol monolayers on gold surfaces exists[13,14]. Of the 20 naturally occurring amino acids, only cysteine (HS-CH_2-$CH(NH_2)$-COOH) contains a mercapto substituent, making this chiral amino acid interesting for studying adsorption on gold surfaces.

Schematic illustrations of the structural features of the amino acid and the gold surface used in this study are given in Fig. 1a and b. Figure 1c shows a scanning tunnelling microscope (STM) image of the gold surface with a low density of adsorbed L-cysteine molecules. The deposition of cysteine leads to the formation of bright protrusions at the sides of the close-packed gold atom rows. The protrusions always exist as pairs, and we ascribe each of the protrusions to an individual cysteine molecule. We have not observed any unpaired protrusions that could be interpreted as isolated molecules.

The main axis running through the two bright lobes of these characteristic double-lobe features is always rotated 20 degrees clockwise with respect to the close-packed [1$\bar{1}$0] direction. The adsorbed cysteine pairs thus break the mirror symmetry of the gold surface. When the mirror-image form of the molecules, D-cysteine, is deposited, we observe similar molecular pairs, but these are rotated 20 degrees anticlockwise with respect to the [1$\bar{1}$0] surface direction (Fig. 1d). The breaking of the mirror symmetry of the gold surface must therefore result from the chirality of the cysteine molecules themselves, with the STM measurements allowing us to identify the chiral conformation of individual, enantiomerically pure molecular pairs[3,4].

When depositing a racemic mixture of cysteine onto the gold surface, we observe molecular dimers (see Fig. 1e) identical to those seen in the previous measurements using pure enantiomers, that is, they are either of the LL form (rotated clockwise) or of the DD form (rotated anticlockwise). New structures that could be ascribed to the pairing of molecules of opposite chirality are not observed. This result suggests that the dimerization of the cysteine molecules is highly stereoselective, with each molecule binding exclusively to partners that have an identical enantiomeric form.

The binding of the cysteine pairs to the gold surface is accompanied by the removal of gold atoms from the close-packed rows. This is evidenced by images acquired under special, accidental tip conditions where the molecular dimers become transparent, showing underlying holes in the surface (Fig. 2a). We gauge that each

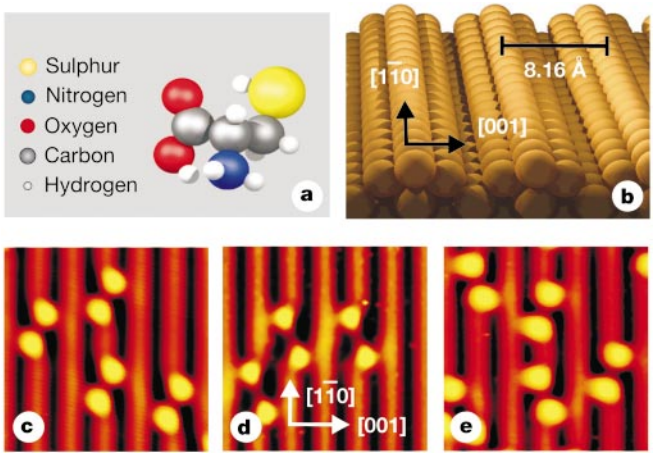

Figure 1 Schematic drawings of a cysteine molecule and the gold (110) surface, and STM images of cysteine pairs on gold (110). **a**, Schematic drawing of a cysteine molecule. **b**, Ball model of the Au(110) surface, which reconstructs into a characteristic missing row structure with every second close-packed row being removed, resulting in a (1 × 2) surface unit cell. **c**, STM image of L-cysteine pairs. The double-lobe, bright protrusions have a linear extent of 7 Å and are separated by a centre-to-centre distance of 9 Å. The main axis of the cysteine pair is rotated 20 degrees clockwise (49 Å × 53 Å). **d**, D-cysteine pairs rotated anticlockwise (same size). The difference in appearance of this image compared with Fig. 1c is ascribed to a slight change in tip condition. **e**, Molecular pairs formed from DL-cysteine (same size).

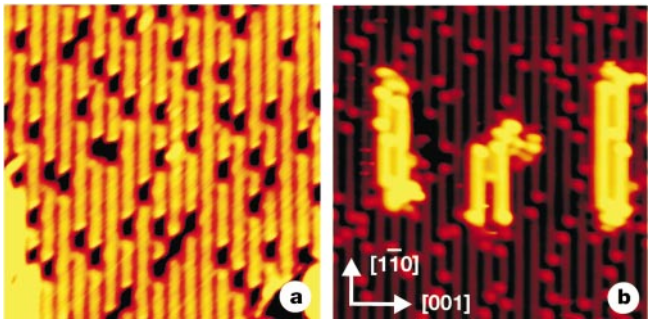

Figure 2 STM images showing absorbate-induced removal of gold atoms. **a**, In STM images obtained under special tip conditions, the molecular dimers appear transparent and the underlying Au substrate is imaged instead. In these circumstances holes, which lack the characteristic off-axis rotation of the molecules, appear along the gold close-packed rows (163 Å × 177 Å). **b**, Terrace after DL-cysteine deposition. Added gold islands are formed by the removed gold atoms (same size).

cysteine dimer covers four atomic vacancies in the underlying close-packed row. The ejected gold atoms nucleate and grow into islands on extended gold terraces, as shown in Fig. 2b. The activation energy needed to achieve vacancies in the gold surface qualitatively explains why the pairs only form after annealing (see Methods section).

To understand the origin of the observed chiral recognition, we have performed *ab initio* density-functional theory (DFT) calculations[10]. Starting with pairs of cysteine molecules interacting in the gas phase, we find stable bimolecular complexes held together through (1) single or double OH–O hydrogen bonds formed between carboxylic groups on the two molecules, (2) one or two OH–N hydrogen bonds formed between carboxylic and amino groups, or (3) an S–S bond between two cysteinates (-S-CH_2-CH(NH_2)-COOH). The interaction involving the carboxylic groups leads to the most stable configuration, and we therefore focus our calculations on this configuration. We also draw upon the general knowledge[13,14,16] that thiols at Au surfaces undergo dissociation to thiolates, followed by binding to the surface through a S–Au bond.

The most favourable adsorption configuration calculated for an LL dimer adsorbed on a four-atom-vacancy structure in the gold rows is shown in Fig. 3a. For comparison, the figure also shows a simulated STM image of this LL dimer. (The image is simulated using the simple Tersoff–Hamann[17] model, where the tunnel current is proportional to the local density of states at the Fermi level projected to the tip apex.) Distinct, bright lobes are found over each of the molecules, in agreement with the experimental STM image (Fig. 1c). Because D- and L-cysteine are related by mirror symmetry, a DD dimer is formed by mirroring of the LL dimer in the (001) crystal plane through the gold close-packed row, yielding an STM image in accordance with the experimental DD dimer image (Fig. 1d).

The preference of the sulphur to bind to low-coordinated gold atoms leads to the formation of vacancies in the gold rows. The optimum adsorption site for the sulphur headgroup is the bridge site[18], so the LL dimer rotates off the direction of the close-packed rows, allowing both sulphur atoms in the dimer to bind at bridge sites between the first and second layer of gold atoms. The calculations also show that the clockwise rotation of the LL dimer enables bond formation between the lone-pairs of the two amino groups and the gold surface, thus further stabilizing this structure.

Possible DL dimer configurations can conveniently be formed by changing one of the L-cysteine molecules in the LL dimer into D-cysteine, thus allowing us to explore why heterochiral dimers do not form. The simplest such substitution is shown in Fig. 3b, where the hydrogen atom and amino group are interchanged on the asymmetric carbon of one of the molecules. This preserves the strong S–Au and carboxylic–carboxylic bonds, while one of the two (weaker) amino–gold bonds is lost. Consequently, the DL dimer in Fig. 3b is calculated to be energetically less stable than the homochiral dimers by around 0.2 eV. This energy cost is of the order of the amino–gold interaction energy and sufficient to suppress the formation of the DL dimer, explaining why we do not observe STM images of asymmetric dimers such as simulated in Fig. 3b. Another DL dimer is formed by mirroring one of the molecules of the LL dimer through the (001) plane. Such a construction introduces a mismatch in the strong carboxylic–carboxylic bond; this bond reforms when relaxing the dimer structure, but only at the expense of breaking both amino–gold bonds (the N–Au separations are expanded from 2.4 to 2.7 Å). This DL dimer (Fig. 3c) is about 0.5 eV less stable than the LL dimer, again

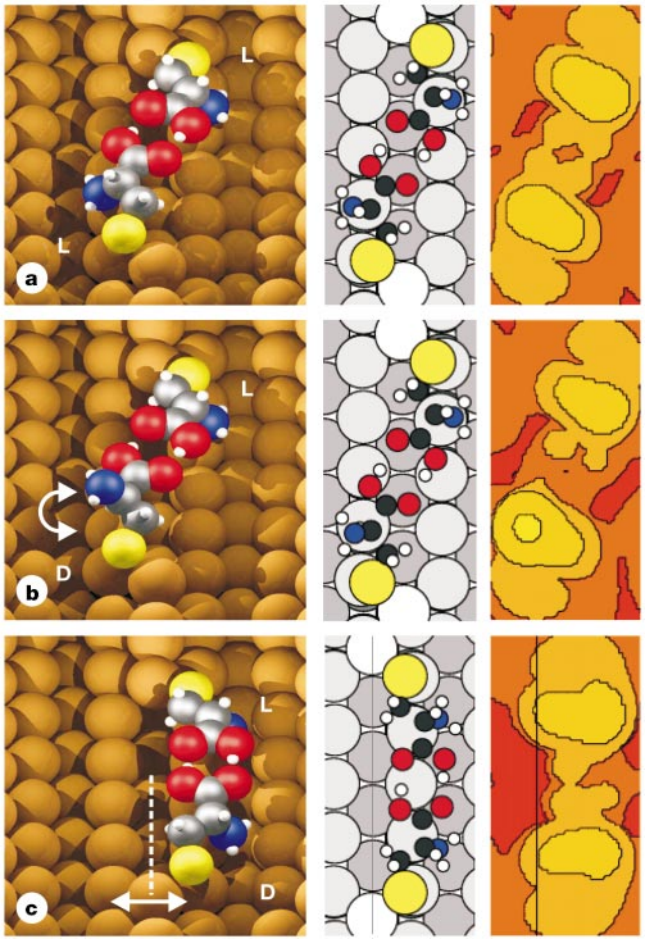

Figure 3 DFT results for cysteine pairs on the Au(110) surface. Large circles represent gold atoms. Small white, black, blue, red and yellow circles represent hydrogen, carbon, nitrogen, oxygen and sulphur atoms, respectively. **a**, An LL-cysteine dimer in three-dimensional and top view as well as the simulated STM image showing the surface of constant local density of states. The contours of constant height are separated by 1.0 Å. **b**, Geometry for a DL dimer obtained by interchanging the amino group and the hydrogen atom on the asymmetric carbon atom. The simulated STM image shows an asymmetric dimer. **c**, DL dimer obtained by mirroring one cysteine molecule in the plane indicated by the dashed line, followed by computational relaxation. The simulated STM image of this dimer shows both lobes on the same side of the close-packed row.

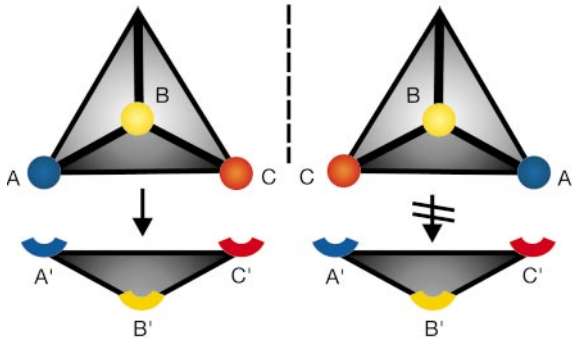

Figure 4 Illustration of the three-point contact model for enantioselectivity in intermolecular interactions. The molecule on the left with contact points A, B and C matches the corresponding receptor sites A′, B′ and C′. The mirror-imaged enantiomeric form of the molecule (right) does not match this receptor, thereby enabling chiral discrimination.

explaining why the simulated STM image is not observed experimentally.

The DFT studies indicate that the preferred formation of homochiral dimers is driven by the optimization of three bonds on each cysteine molecule (sulphur–gold, amino–gold, and carboxylic–carboxylic). By directly pin-pointing the three bonds involved in the chiral recognition process, our results constitute a direct molecular-level demonstration of the generic, conceptual three-point contact model[11,12] for chiral recognition, illustrated in Fig. 4. Furthermore, the results indicate that the surface and the local surface restructuring help to facilitate the chiral interaction. This is likely to be fundamentally relevant for the field of heterogeneous enantiospecific catalysis. □

Methods

The experiments were performed in an ultrahigh vacuum system equipped with a home-built STM[19]. Cysteine molecules were transferred to the Au(110)-(1×2)[15] surface by vapour deposition onto a sample held at room temperature, leading to the formation of compact agglomerates of cysteine molecules. The dilute cysteine dimer structure reported upon here was obtained by annealing to 340 K for 15 minutes, leading to dissolution of the agglomerates and formation of the molecular pairs. All STM observations were performed at room temperature.

The DFT calculations[10], including full structural optimization using the non-local density gradient approximation[20], were done with 38 independent gold atoms arranged in a slab geometry modelling four layers of the reconstructed gold (110) surface. The upper two layers of gold atoms and all of the 26 atoms in the dehydrogenated cysteine dimers were relaxed until the total residual force was below 0.4 eVÅ^{-1}.

Received 11 June; accepted 20 December 2001.

1. Sheldon, R. A. *Chirotechnology* 39–72 (Dekker, New York/Basel, 1993).
2. Cline, D. B. *Physical Origin of Homochirality in Life* 17–49 (AIP Press, Woodbury, New York, 1996).
3. Fang, H., Giancarlo, L. C. & Flynn, G. W. Direct determination of the chirality of organic molecules by scanning tunneling microscopy. *J. Phys. Chem.* **102,** 7311–7315 (1998).
4. Lopinski, G. P., Moffatt, D. J., Wayner, D. D. M. & Wolkow, R. A. Determination of the absolute chirality of individual adsorbed molecules using the scanning tunneling microscope. *Nature* **392,** 909–911 (1998).
5. Böhringer, M., Morgenstern, K., Schneider, W.-D. & Berndt, R. Separation of a racemic mixture of two-dimensional molecular clusters by scanning tuneling microscopy. *Angew. Chem. Int. Edn* **38,** 821–823 (1999).
6. McKendry, R., Theoclitou, M.-E., Rayment, T. & Abell, Ch. Chiral discrimination by chemical force microscopy. *Nature* **391,** 566–569 (1998).
7. Lorenzo, M. O., Baddeley, C. J., Muryn, C. & Raval, R. Extended surface chirality from supramolecular assemblies of adsorbed chiral molecules. *Nature* **404,** 376–379 (2000).
8. Chen, Q., Lee, C. W., Frankel, D. J. & Richardson, N. V. The formation of enantiospecific phases on a Cu{110} surface. *PhysChemComm* [online] **9,** (1999).
9. Eckhardt, C. J. *et al.* Separation of chiral phases in monolayer crystals of racemic amphiphiles. *Nature* **362,** 614–616 (1993).
10. Payne, M. C., Teter, M. P., Allan, D. C., Arias, T. A. & Joannopoulos, J. D. Iterative minimization techniques for *ab initio* total-energy calculations: molecular dynamics and conjugate gradients. *Rev. Mod. Phys.* **64,** 1045–1097 (1992).
11. Easson, L. H. & Stedman, E. Studies on the relationship between chemical constitution and physiological action. *Biochem.* **27,** 1257–1266 (1933).
12. Booth, T. D., Wahnon, D. & Wainer, I. W. Is chiral recognition a three-point process? *Chirality* **9,** 96–98 (1997).
13. Ulman, A. Formation and structure of self-assembled monolayers. *Chem. Rev.* **96,** 1533–1554 (1996).
14. Poirier, G. E. & Pylant, E. D. The self-assembly mechanism of alkanethiols on Au(111). *Science* **272,** 1145–1148 (1996).
15. Gritsch, T., Coulman, D., Behm, J. R. & Ertl, G. A. A scanning tunneling microscopy investigation of the structure of the Pt(110) and Au(110) surfaces. *Surf. Sci.* **257,** 297–306 (1991).
16. Grönbeck, H., Curioni, A. & Andreoni, W. Thiols and disulfides on the Au(111) surface: the headgroup-gold interaction. *J. Am. Chem. Soc.* **122,** 3839–3842 (2000).
17. Tersoff, J. & Hamann, D. R. Theory of the scanning tunneling microscopy. *Phys. Rev. B* **31,** 805–813 (1985).
18. Gottschalck, J. & Hammer, B. A density functional theory study of the adsorption of sulfur, mercapto and methylthiolate on Au(111). *J. Chem. Phys.* **116,** 784–790 (2002).
19. Lægsgaard, E., Besenbacher, F., Mortensen, K. & Stensgaard, I. A fully automated, 'thimble-size' scanning tunnelling microscope. *J. Microscopy* **152,** 663–669 (1988).
20. Perdew, J. P. *et al.* Atoms, molecules, solids, and surfaces: Applications of the generalized gradient approximation for exchange and correlation. *Phys. Rev. B* **46,** 6671–6687 (1992).

Acknowledgements

This work was supported by the Danish National Research Foundation through the Center for Atomic-scale Materials Physics (CAMP) and by the Danish Natural Science Research Council.

Correspondence and requests for materials should be addressed to F.B. (e-mail: fbe@ifa.au.dk).

Deterioration of the seventeenth-century warship *Vasa* by internal formation of sulphuric acid

Magnus Sandström*, Farideh Jalilehvand†, Ingmar Persson‡, Ulrik Gelius§, Patrick Frank†¶ & Ingrid Hall-Roth#

** Department of Structural Chemistry, University of Stockholm, SE-106 91 Stockholm, Sweden*
† Stanford Synchrotron Radiation Laboratory, SLAC, Stanford University, PO Box 4349, MS 69, Stanford, California 94309, USA
‡ Department of Chemistry, Swedish University of Agricultural Sciences, PO Box 7015, SE-750 07 Uppsala, Sweden
§ Department of Physics, Ångström Laboratory, Uppsala University, PO Box 530, SE-751 21 Uppsala, Sweden
¶ Department of Chemistry, Stanford University, Stanford, California 94305, USA
 # The Vasa Museum, PO Box 27131, SE-102 52, Stockholm, Sweden

The seventeenth-century Swedish warship, *Vasa*, was recovered in good condition after 333 years in the cold brackish water of Stockholm harbour. After extensive treatment to stabilize and dry the ship's timbers[1], the ship has been on display in the Vasa Museum since 1990. However, high acidity and a rapid spread of sulphate salts were recently observed on many wooden surfaces[2], which threaten the continued preservation of the *Vasa*. Here we show that, in addition to concentrations of sulphate mostly on the surface of oak beams, elemental sulphur has accumulated within the beams (0.2–4 per cent by mass), and also sulphur compounds of intermediate oxidation states exist. The overall quantity of elemental sulphur could produce up to 5,000 kg of sulphuric acid when fully oxidized. We suggest that the oxidation of the reduced sulphur—which probably originated from the penetration of hydrogen sulphide into the timbers as they were exposed to the anoxic water—is being catalysed by iron species released from the completely corroded original iron bolts, as well as from those inserted after salvage. Treatments to arrest acid wood hydrolysis of the *Vasa* and other wooden marine-archaeological artefacts should therefore focus on the removal of sulphur and iron compounds.

The *Vasa* sank in Stockholm harbour on her maiden voyage in 1628, and was salvaged in 1961. The massive oak beams were seemingly in good condition after 333 years at 32 m depth (see http:///www.vasamuseet.se/indexeng.html and links therein). Marine burial occasionally deposits wooden objects in near anoxic environments that arrest natural decay. This favours sulphate-reducing bacteria producing hydrogen sulphide in an environment inhospitable to most wood-metabolizing microbes[3]. In such conditions slow biodegradation of waterlogged wood takes

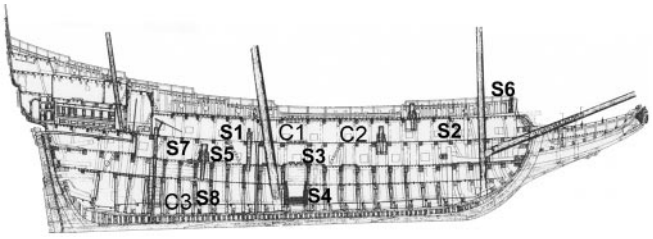

Figure 1 Outline of the hull of the *Vasa* with sample positions indicated. C1–C3, for cores; S1–S8, surface XRD samples. Dimensions: length 61 m (69 m including bowsprit), maximum width 11.7 m, stern castle 19.3 m high, displacement 1,210 tons.